Cell Death Discovery

https://doi.org/10.1038/s41420-026-02958-7

Article in Press

PDHA1 enhances resistance to ferroptosis in anoikis-resistant prostate cancer by upregulating AIFM2

Received: 9 June 2025

Revised: 12 December 2025

Accepted: 9 February 2026

Cite this article as: Cong, Y., Chen, K., Ju, Y. *et al.* PDHA1 enhances resistance to ferroptosis in anoikis-resistant prostate cancer by upregulating AIFM2. *Cell Death Discov.* (2026). https://doi.org/10.1038/s41420-026-02958-7

Yukun Cong, Kang Chen, Yunjie Ju, Qingliu He, Chunyu Liu, Jiawei Chen, Fang Lv, Jinyu Chen, Haoran Li, Liang Chen & Yarong Song

`

PDHA1 enhances resistance to ferroptosis in anoikis resistance prostate cancer by upregulating AIFM2

Yukun Cong[1, 3], Kang Chen[1, 3], Yunjie Ju[1, 3], Qingliu He[1,2], Chunyu Liu[1], Jiawei Chen[1], Fang Lv[1], Jinyu Chen[1], Haoran Li[1*], Liang Chen[1*] and Yarong Song[1*]

[1]Department of Urology, Union Hospital, Tongji Medical College, Huazhong University of Science and Technology, Wuhan 430022, China.

[2]Department of Urology, The Second Affiliated Hospital of Fujian Medical University, Quanzhou 362000, China.

[3]These authors contributed equally

[*]Corresponding authors: Haoran Li (e-mail: lhrslay8868@163.com); Liang Chen (e-mail:2023xh0053@hust.edu.cn); Yarong Song（e-mail:tjmusong@126.com)

Running title: Anti-ferroptosis of PDHA1 in prostate cancer

`

Abstract

Cells that detach from the extracellular matrix (ECM) undergo various forms of cell death, including ferroptosis. Previous studies have demonstrated that prostate cancer (PCa) cells undergo ferroptosis following ECM detachment, and resistance to ferroptosis may facilitate tumor metastasis. Pyruvate dehydrogenase E1 alpha 1 (PDHA1) has been identified as a key regulator in the progression of several malignancies; however, its role in ferroptosis and prostate cancer metastasis remains unclear. In this study, anoikis resistance (AnoR) prostate cancer cells exhibited a substantial increase in PDHA1 expression, which enhanced their survival and metastatic potential by increasing resistance to ferroptosis. Mechanistically, nuclear PDHA1 in AnoR cells facilitated histone H3 lysine 9 acetylation (H3K9Ac) that significantly accumulated at the promoter region of peroxisome proliferator-activated receptor alpha (PPARA), thereby upregulating its expression. PPARA, in turn, activated the transcription of apoptosis-inducing factor mitochondria-associated 2 (AIFM2), whose upregulation inhibited ferroptosis in AnoR prostate cancer cells. This study demonstrates that PDHA1 expression is found to be elevated in primary tumors from patients with metastatic prostate cancer. Additionally, the aberrant overexpression of PDHA1 in AnoR prostate cancer cells upregulates PPARA and AIFM2 expression through nuclear translocation, collectively suppressing ferroptosis and promoting metastasis. These findings reveal a novel role for PDHA1 in mediating ferroptosis resistance during ECM detachment and provide a potential therapeutic target for prostate cancer treatment.

KEYWORDS: prostate cancer; metastasis; PDHA1; ferroptosis; anoikis resistance

`

INTRODUCTION

Prostate cancer ranks as the second most common malignancy among the global male population and represents the fifth leading cause of cancer-related deaths in men. In 2022, approximately 1.5 million new cases and 397,000 PCa-related deaths were reported worldwide [1]. Despite advancements in its diagnosis and treatment in recent years, metastasis remains the principal cause of mortality in PCa, posing significant social and economic burdens [2]. Therefore, elucidating the molecular mechanisms underlying prostate cancer metastasis and identifying effective therapeutic targets have become critical priorities in clinical prostate cancer treatment [3].

Tumor metastasis is a complex process that has several stages: detachment of tumor cells from the primary lesion, dissemination via the circulatory system, and colonization at distant organs [4]. Because the circulatory system lacks an extracellular matrix (ECM), cells that detach from the ECM undergo a specific type of programmed cell death known as anoikis [5]. Anoikis resistance (AnoR), which allows tumor cells to survive and disseminate through vascular and lymphatic systems, is a crucial prerequisite for metastasis [6-8]. Ferroptosis, a newly identified type of regulated cell death (RCD), is driven by iron-dependent lipid peroxidation of polyunsaturated fatty acid phospholipids [8,9] and can be triggered by erastin, a selective lethal compound [10]. Widely regarded as a regulated cell death mechanism, ferroptosis has also been shown in recent studies to be implicated in tumor cell death after detachment from ECM [5,6]. Moreover, ferroptosis is tightly regulated at multiple levels, including epigenetic modifications, **s**uch as histone acetylation [11]. Histone acetylation neutralizes the positive charge on lysine residues, thereby facilitating gene transcription activation. Histone H3 lysine 9 acetylation (H3K9Ac) is widely recognized as a hallmark of gene activation, playing a crucial role in transcription initiation and elongation [12]. Research has shown that cell division cycle 25A (Cdc25A)

`

upregulates ErbB2 expression via the PKM2-pH3T11-H3K9Ac pathway, thereby protecting cervical cancer cells from autophagy-mediated ferroptosis [13].

Acetyl-coenzyme A (acetyl-CoA) serves as a crucial substrate for histone acetylation. In eukaryotes cells, due to the membrane impermeability of acetyl-CoA and the instability of its high-energy thioester bond, its biosynthesis is compartmentalized within subcellular organelles, with a unique nuclear mechanism for histone acetylation [14]. As a core intermediate of the carbon source, acetyl-CoA not only generates ATP through the tricarboxylic acid (TCA) cycle but also serves as an essential acetyl donor for lysine acetylation in mammalian cells, which is crucial for cell growth and survival [15]. The pyruvate dehydrogenase complex (PDC) is a multiprotein complex that comprises three enzymatic components—pyruvate decarboxylase (E1), dihydrolipoamide acetyltransferase (E2), and dihydrolipoamide dehydrogenase (E3) [16]. PDC catalyzes the conversion of pyruvate to acetyl-CoA. Pyruvate dehydrogenase (PDH), the initial rate-limiting enzyme in this process, is responsible for the oxidative decarboxylation of pyruvate to produce acetyl-CoA, thereby influencing histone acetylation [17]. Pyruvate dehydrogenase E1 alpha 1 (PDHA1), a catalytic subunit of PDH, is regulated via phosphorylation by pyruvate dehydrogenase kinases (PDKs) and dephosphorylation by pyruvate dehydrogenase phosphatases (PDP1 and PDP2) [18]. Although traditionally regarded as a key player in mitochondrial metabolism, PDHA1 has also been implicated in controlling the nuclear acetyl-CoA pool recently, thereby promoting histone acetylation and influencing gene expression [14]. Additionally, high PDHA1 expression has been found to promote metastasis in other cancers, such as cholangiocarcinoma [19]. While previous studies have demonstrated the pro-metastatic role of PDHA1 and the regulatory function of histone acetylation in ferroptosis and metastasis, the specific regulatory mechanisms of PDHA1 in prostate cancer remain unclear. Therefore, it is imperative to elucidate the potential functions of PDHA1 and histone acetylation

`

in ferroptosis and anoikis resistance in prostate cancer to gain deeper insight into the molecular basis of this disease.

This study systematically examined ferroptosis-associated gene expression and found that apoptosis-inducing factor mitochondria-associated 2 (AIFM2) was significantly impacted by PDHA1. We demonstrated that in AnoR PCa cells, PDHA1 enhances core histone acetylation through extensive nuclear translocation, subsequently enriching H3K9Ac within the peroxisome proliferator-activated receptor alpha (PPARA) promoter region. This process upregulated the expression of PPARA and AIFM2. Animal models corroborated that targeting the PDHA1-AIFM2 axis enhanced the suppression of AnoR PCa progression. Collectively, these findings reveal a novel checkpoint in ferroptosis resistance in prostate cancer and suggest that enhancing ferroptosis might be a strategy for improving anti-tumor efficacy.

RESULTS

PDHA1 is highly expressed in AnoR PCa cells and correlates with PCa metastasis and prognosis

To further investigate the relationship between PDHA1 and anoikis resistance, we cultured parental PC-3 and 22Rv1 cells in ultra-low-attachment six-well plates, thereby creating an AnoR cell model to simulate anoikis resistance. Previous studies have shown that AnoR cells exhibit greater migratory and invasive capacities compared with their parental counterparts [21]. In addition, our findings indicate that AR cells also display enhanced viability (Supplementary Fig. 1A). Western blot revealed a significant increase in PDHA1 protein expression in AnoR PCa cells compared with their parental（P）cells (Fig. 1A). PDH activity was also stronger in AnoR cells (Fig. 1B). Previous studies have demonstrated that PDHA1, the catalytic subunit of the PDH complex, directly determines PDH activity [20]; therefore, an increase in PDH activity indicates elevated PDHA1 expression. Bioinformatics analysis of the MCTP cohort using the cBioPortal for

`

Cancer Genomics (http://cbioportal.org) showed that PDHA1 expression was significantly upregulated in the primary tumors of metastatic prostate cancer patients compared to those without metastasis (Fig. 1C). For further validation, we collected prostate cancer primary lesions from 10 patients negative for lymph node metastasis (N0) and 10 patients positive for lymph node metastasis (N1). Immunohistochemical assays revealed higher PDHA1 expression in the prostate tumor tissues from patients with lymph node metastasis (Fig. 1D-E). Western blot results were consistent with findings of the Immunohistochemical assays (Fig. 1 F-G). Moreover, analysis of The Cancer Genome Atlas (TCGA) database indicated an association between elevated PDHA1 expression and disease-free survival (DFS), Gleason score and lymph node metastasis (Supplementary Fig. 1B-D). A further transwell assay showed that PDHA1 knockdown significantly reduced the migration and invasion of AnoR PCa cells (Fig.1H-K), and overexpression of PDHA1 promoted migration and invasion (Supplementary Fig. 1E-G). Additionally, Wound healing assay demonstrated that PDHA1 knockdown significantly reduced metastasis of AnoR PC-3 cells (Fig. 1L-M and Supplementary Fig. 1H-I), whereas overexpression of PDHA1 produced the opposite effect (Supplementary Fig. 1J-L). Collectively, these findings indicate that PDHA1 is highly expressed in AnoR PCa cells, and its high expression is closely correlated with prostate cancer metastasis and prognosis.

PDHA1 promotes ferroptosis resistance in AnoR PCa cells

Previous studies have shown that inactivation of PDHA1 can inhibit the proliferation of prostate cancer cells [22]. Additionally, ferroptosis, a form of programmed cell death characterized by iron-dependent lipid peroxidation, plays an important role in the death process of tumor cells following detachment from the extracellular matrix (ECM) [21,23]. Given these observations, we hypothesized a link between PDHA1,

`

ferroptosis, and anoikis resistance. We first performed CCK-8 assays to monitor changes in cell viability following treatment with various cell death inhibitors, including Z-VAD (apoptosis inhibitor), Disulfiram (pyroptosis inhibitor), Necrostatin-2 (necroptosis inhibitor), and Ferrostatin-1 (ferroptosis inhibitor), either alone or in combination with Erastin (ferroptosis inducer). Stable downregulation of PDHA1 in AnoR PC-3 cells treated with Erastin showed a significant decrease in cell viability, which was reversed by Ferrostatin-1. However, the Z-VAD, Disulfiram, and Necrostatin-2 did not significantly reverse this decreasing effect. A similar effect was observed in AnoR 22Rv1 cells (Fig. 2A). Subsequently, we utilized the TCGA database to categorize patients into two groups based on high and low PDHA1 expression levels and conducted gene set enrichment analysis (GSEA). The analysis indicated a significant association between elevated PDHA1 expression and the reactive oxygen species (ROS) pathway (Fig. 2B). Since reduced ROS levels are known to inhibit ferroptosis [24], we assessed ROS levels and observed that ROS levels were markedly increased in AnoR PCa cells with stable PDHA1 knockdown (Fig. 2C and Supplementary Fig. 2A). Conversely, overexpression of PDHA1 in AnoR PCa cells resulted in a decreased ROS level (Supplementary Fig. 2B). Additionally, further investigation of ferroptosis-related indicators revealed that PDHA1 downregulation significantly reduced mitochondrial membrane potential (MMP) levels in AnoR PC-3 cells (Fig. 2D) and AnoR 22Rv1 cells (Supplementary Fig. 2C). Additionally, downregulated PDHA1 led to a significantly elevated MDA level in AnoR PCa cells (Fig. 2E), while overexpression exerted a diametrically opposite effect (Supplementary Fig. 2D). Following PDHA1 knockdown, lipid reactive oxygen species levels were markedly elevated, whereas intracellular iron levels showed no significant change (Fig. 2F-G and Supplementary Fig. 2E-F).

`

Transmission electron microscopy (TEM) revealed that AnoR PC-3 and 22Rv1 cells with PDHA1 knockdown exhibited significantly smaller mitochondria, shorter or complete disappearance of mitochondrial cristae, and increased membrane density (Fig. 2H and Supplementary Fig. 2G). Moreover, evidence showed that inhibition of ferroptosis promoted metastasis in gastric and breast cancers [25,26]. Combining these findings with previous studies, we concluded that PDHA1 can promote anoikis resistance and tumor metastasis in PCa by inhibiting ferroptosis.

PDHA1 inhibits ferroptosis of AnoR PCa cells by upregulating AIFM2

To investigate how PDHA1 upregulation inhibits ferroptosis, we analyzed ferroptosis-related genes that could be affected by PDHA1 in AnoR PCa cells, including SLC3A2, GPX4, ACSL4, SLC7A11, DHODH, and AIFM2 [27-32]. Western blot analysis showed that AIFM2 levels were significantly elevated in AnoR PC-3 and 22Rv1 cells with stable PDHA1 overexpression. In contrast, the expression of other related proteins (SLC3A2, GPX4, ACSL4, SLC7A11 and DHODH) was not affected. Knockdown of PDHA1 resulted in a reduction of AIFM2 levels, without affecting other related proteins (Fig. 3A and Supplementary Fig. 3A). Correlation analysis of expression levels in prostate cancer specimens from the TCGA PRAD database revealed a significant association between PDHA1 and AIFM2 expression (Supplementary Fig. 3B). We subsequently investigated the relationship between AIFM2 and prostate cancer metastasis. Bioinformatic analysis using the cBioPortal MCTP cohort and TCGA database showed that AIFM2 expression was elevated in primary lesions of metastatic prostate cancer patients (Fig. 3B) and an association between elevated PDHA1 expression and pathological N stage (Supplementary Fig. 3D). Additionally, AIFM2 expression was found to be higher in prostate cancer tissues with lymph node metastasis compared to those without lymph node metastasis (Fig.

`

3C-D). Further validation by west blot analysis revealed that the expression level of AIFM2 was higher in PCa with lymph-node metastasis compared to their counterparts without (Fig. 3E). These findings collectively suggest that AIFM2 serves as a key downstream effector of PDHA1 in inhibiting ferroptosis and promoting prostate cancer metastasis.

Subsequently, Western blot analysis demonstrated that overexpression of AIFM2 reversed the effects of PDHA1 knockdown, whereas knockdown of AIFM2 counteracted the effects of PDHA1 overexpression, confirming that AIFM2 is regulated by PDHA1 (Fig. 3F and Supplementary Fig. 3C). In CCK-8 experiments, we observed that AIFM2 overexpression promoted cancer cell survival, while PDHA1 knockdown suppressed it (Fig. 3G and Supplementary Fig. 3E). Overexpression of AIFM2 inhibited the levels of ferroptosis-related indicators triggered by PDHA1 downregulation including MDA (Supplementary Fig. 3G), MMP (Fig. 3H and Supplementary Fig. 3F), lipid reactive oxygen species (Fig. 3I and Supplementary Fig. 3H) and ROS (Fig. 3J) in AnoR PC-3 and 22Rv1 cells. Collectively, these findings suggest that increased PDHA1 inhibits ferroptosis by promoting AIFM2 expression.

AIFM2 rescues progression of PDHA1 knockdown AnoR PCa cells

We performed in vitro and in vivo experiments to assess if PDHA1 exerts its biological effects via AIFM2. Transwell assays demonstrated that AIFM2 overexpression significantly enhanced the migration and invasion of AnoR PC-3 and 22Rv1 cells. Conversely, PDHA1 knockdown reduced their migration and invasion, and these effects were reversed by AIFM2 overexpression, thereby enhancing metastatic potential (Fig. 4A-D). Wound healing assay demonstrated that upregulation of AIFM2 restored the lowered cellular metastasis induced by PDHA1 downregulation (Fig. 4E-H).

`

To validate these findings in vivo, we developed a lung metastasis model by injecting red fluorescent AnoR PC-3 cells into the tail vein of nude mice. Consistent with the aforementioned results, bioluminescent imaging exhibited that PDHA1 knockdown significantly reduced the number and size of lung metastatic tumors, and we observed a greater survival probability in mice in vivo experiment. However, AIFM2 overexpression significantly counteracted the effect of PDHA1 knockdown, resulting in an increase in the number and size of lung metastatic tumors and a decrease in survival probability (Fig. 4I-J). These findings confirmed that the downregulation of PDHA1 inhibited the progression of AnoR PCa cells by reducing AIFM2 expression, both in vitro and in vivo.

PDHA1 promotes downstream gene expression by translocating into the nucleus to regulate histone acetylation

Recent studies indicated that PDHA1 could regulate nuclear acetyl-CoA levels in the cell nucleus, thereby influencing H3K9 acetylation (H3K9Ac) [16]. Based on this evidence, we used immunofluorescence and protein fractionation techniques to analyze PDHA1 localization. We found nuclear localization of PDHA1 was stronger in AnoR cells compared to their parental counterparts (Fig. 5A, B). Subsequent analysis of intracellular H3K9Ac levels revealed higher levels in AnoR PCa cells than in parental cells (Fig. 5D). Notably, knocking down PDHA1 in AnoR PCa cells decreased the H3K9Ac level, while overexpression of PDHA1 increased it (Fig. 5C), potentially affecting gene expression.

Cellular compartmentalization enables the concurrent execution of distinct metabolic reactions, and aberrant protein compartmentalization has been linked to cancer development [33]. To verify whether PDHA1 regulates histone acetylation level by translocating into the nucleus, we investigated the role of nuclear PDHA1 in AnoR PCa cells by expressing nuclear localization

`

signaling fusion PDHA1 (NLS-PDHA1) and mutated NLS sequences (NLS-PDHA1-mut) vectors in AnoR PCa cells previously infected with short hairpin RNA of PDHA1 (shPDHA1) (Fig. 5E, F and Supplementary Fig. 3I). Functional validation revealed that mutation of these NLS motifs markedly reduced the nuclear accumulation of PDHA1, thereby supporting the functional relevance of the identified NLS sequences in mediating nuclear import. We observed that reintroducing NLS-PDHA1 into shPDHA1 cells restored H3K9Ac and ferroptosis-related gene AIFM2 expression (Fig. 5G). These results suggest that PDHA1 regulates the expression of ferroptosis-related genes autonomously by translocating into the nucleus. Interestingly, after we utilized UCSC (http://genome.ucsc.edu/) and the Cistrome database (http://cistrome.org/db/) to predict the H3K9Ac binding site on the AIFM2 promoter (Supplementary Fig. 4E), we observed via ChIP-PCR that the increased histone acetylation level induced by overexpression of PDHA1 did not directly influence AIFM2 expression changes (Fig. 5H). In addition, the co-immunoprecipitation (Co-IP) results for PDHA1 and AIFM2 indicated that there was no direct interaction between the two proteins (Supplementary Fig. 3J). We therefore postulated that the relationship between PDHA1 and AIFM2 expression might be mediated by other molecules.

PDHA1 upregulates AIFM2 expression by promoting transcriptional activation of PPARA

To investigate the mechanism of PDHA1 regulating AIFM2 expression, we utilized the Gene Expression Omnibus (GEO) dataset (GEO accession: GSE100629) and identified 2,370 differentially expressed genes in AnoR cells, of which 1,183 were upregulated (Log2FC > 1, $p < 0.05$). Given that H3K9Ac generally promotes transcriptional activation [34], we cross-referenced these upregulated genes with the genes that inhibited ferroptosis in FerrDb V2 database (http://www.zhounan.org/ferrdb) of and identified 13 genes (Fig. 6A). Subsequently, qRT-PCR showed that overexpression of PDHA1 resulted in the most significant change in PPARA expression among these 13 genes (Fig. 6B). This was further verified by Western blot analysis, showing that

`

knockdown of PDHA1 decreased PPARA expression, while overexpression of PDHA1 increased it (Supplementary Fig. 4A). Similarly, we used the TCGA database to divide the patients into two groups based on high and low PDHA1 expression and conducted a gene set enrichment analysis (GSEA). The analysis revealed a significant correlation between high PDHA1 expression and the peroxisome pathway (Supplementary Fig. 4B). To further validate the role of PPARA in metastasis, we evaluated the pharmacological inhibition of PPARA using GW6471, and the results demonstrated that GW6471 treatment significantly suppressed the metastatic capacity of prostate cancer cells (Supplement Fig. 4C). The IHC analysis revealed that the expression level of PPARA was higher in the prostate tissues of patients with lymph node metastasis compared to their counterparts without (Fig. 6C). These findings indicate that pharmacological inhibition of PPARA effectively suppresses the metastatic potential of prostate cancer cells, supporting the functional relevance of the PDHA1–PPARA–AIFM2 axis in regulating tumor progression.

Additionally, expressing NLS-PDHA1 in AnoR PCa cells infected with shPDHA1 increased PPARA expression compared with cells not expressing NLS-PDHA1 (Fig. 6D).

To verify whether PPARA is a mediator of PDHA1 regulation of AIFM2, we first utilized the UCSC and Cistrome databases to predict whether H3K9Ac binding sites on the PPARA promoter (Supplementary Fig. 4D). ChIP-PCR confirmed that PDHA1 modulates PPARA expression by regulating H3K9Ac enrichment at its promoter (Fig. 6E). The results suggested that PDHA1 nuclear translocation influences H3K9Ac levels and subsequently regulates PPARA expression.

PPARA is a key transcription factor in large-scale reorganization of lipid homeostasis [35] and had been reported to transcriptionally activate SLC47A1 expression to regulate ferroptosis [36]. Therefore, we examined whether PPARA influenced AIFM2 expression through its transcriptional activity. Using the hTFtarget database (http://bioinfo.life.hust.edu.cn/hTFtarget), we predicted potential PPARA binding sites on the AIFM2 promoter (Fig.6F and Supplementary Fig. 4F). A dual-luciferase reporter plasmid containing the wild-type (wt) AIFM2 promoter was constructed and transfected into AnoR PC-3 and AnoR 22Rv1 cells to assess the transcriptional activity of PPARA. Overexpression of PPARA significantly enhanced luciferase activity relative to the control vector

`

(Fig. 6G).

To further explore how PPARA regulates AIFM2 transcription, we constructed the dual-luciferase reporter plasmid with the mutated AIFM2 promoter. Our findings revealed that PPARA's capacity to activate AIFM2 transcription was substantially diminished only when transcription factor binding site 1 (TFBS1) was altered, while mutations at other sites had no similar effect (Fig. 6H). Moreover, when all binding sites were mutated, the results mirrored those seen with the TFBS1 mutation alone (Supplementary Fig. 4G). Therefore, we concluded that PPARA enhances AIFM2 expression specifically through TFBS1. To further confirm that PDHA1 influences AIFM2 via PPARA, rescue experiments were performed. Western blot analysis revealed that PPARA overexpression rescued the decrease in AIFM2 protein levels caused by knockdown of PDHA1 (Fig.6I). Moreover, the overexpression of either PDHA1 or PPARA alone increased AIFM2 expression and relative reporter activity compared to the empty vector control, with a further increase observed when both were overexpressed simultaneously (Fig.6J and Supplementary Fig. 4H). These findings demonstrate that PDHA1 enhances PPARA expression through increased H3K9Ac enrichment, thereby transcriptionally activating AIFM2 (Fig.7).

DISCUSSION

Anoikis resistance is a critical early event in cancer metastasis, enabling cancer cells to survive after detachment from the ECM, enter the vasculature, and disseminate to distant organs. It has been demonstrated to be a prerequisite for hematogenous metastasis [37] and lymphatic metastasis [38]. Understanding the mechanisms underlying anoikis resistance and its connection to prostate cancer metastasis may provide in-depth insights into cancer biology and help identify new therapeutic targets for preventing cancer progression [39,40].

The role of PDC in cancer, whether it act as a pro-tumorigenic or tumor-suppressive factor, remains controversial [41,42,43,44]. In this study, by establishing a detachment resistance model to mimic the anoikis resistance environment, our data provided a new perspective by demonstrating that PDHA1, a subunit of PDC, was upregulated at the protein level in AnoR PCa cells and was active in the nucleus, thereby promoting AnoR PCa cells metastasis and survival. PDHA1 overexpression significantly enhanced the proliferation, migration, and invasion of AnoR PCa cells, whereas PDHA1 knockdown impaired

`

these abilities. Furthermore, high PDHA1 expression was closely associated with worse disease-free survival (DFS), higher Gleason score, and advanced pathological N stage. Based on these data, we propose that increased PDHA1 plays an important role in promoting PCa progression. Thus, our study provides a prospect of targeting PDHA1 for the management of prostate cancer metastasis. Future studies should aim at the development of PDHA1 inhibitors to efficaciously prevent prostate cancer metastasis.

Before metastasizing to distant organs, cancer cells must acquire anoikis resistance to survive in the circulation [45]. Anoikis can occur via an intrinsic pathway resulting from mitochondrial perturbation or an extrinsic pathway triggered by cell surface death receptors [46]. In the intrinsic pathway, ROS generation is markedly increased following detachment, leading to oxidative damage to cellular macromolecules and subsequent cell death [47]. Excessive ROS is also closely associated with ferroptosis, and recent studies have suggested that anoikis-resistant cancer cells exhibit resistance to ferroptosis [48]. Beyond prostate cancer, ferroptosis has been widely recognized as a key determinant of metastatic behavior across diverse malignancies. It not only impacts primary tumor progression but also modulates epithelial–mesenchymal transition and adaptation to metastatic niches [49], thereby shaping the overall metastatic cascade. Collectively, these findings support the concept that targeting ferroptosis may represent a promising therapeutic avenue to prevent or limit cancer metastasis.

By integrating the aforementioned findings, our results suggested that the decreased cell viability induced by Erastin in PDHA1 knockdown AnoR PCa cells was enhanced by Ferrostatin-1 but not by other death inhibitors. At the same time, PDHA1 knockdown and overexpression correspondingly increased or decreased intracellular MMP, lipid reactive oxygen species, ROS and MDA levels, respectively. On the basis of these findings, we propose that PDHA1 plays a role in ferroptosis regulation during ECM detachment in PCa cells. Subsequently, we measured levels of key ferroptosis-related genes and found that PDHA1 regulates the expression of AIFM2. We were led to theorize that PDHA1 might help AnoR PCa cells resist ferroptosis by increasing AIFM2 expression. AIFM2 has been identified as an endogenous ferroptosis inhibitor that exerts an inhibitory effect on lipid peroxidation by lowering CoQ10 with NAD(P)H [50]. It has been

`

shown that AIFM2 promotes hepatocellular carcinoma metastasis by activating mitochondrial SIRT1/PGC-1α signaling [51]. In this study, both in vitro and in vivo experiments demonstrated that AIFM2 overexpression reversed the suppression in metastasis and survival potential of AnoR PCa cells and restored ferroptosis sensitivity induced by PDHA1 knockdown. These findings suggest that PDHA1 promotes AnoR PCa cell metastasis by upregulating AIFM2 expression and suppressing ferroptosis.

Acetylation is one of the post-translational modifications (PTMs) that affects diverse aspects of protein biology [52]. Histone acetylation is associated with transcriptional activation, which weakens histone-DNA interactions by neutralizing the positive charge of lysine, thereby improving chromatin accessibility [53]. In fact, growing evidence indicates that aberrant histone acetylation constitutes one of the pathogenic mechanisms of cancer development. For instance, HMGCL increases β-hydroxybutyrate (β-OHB)-mediated acetylation of DPP4 at histone H3 lysine 9, promoting its expression and resulting in HCC cells being more susceptible to erastin-induced ferroptosis [54]. Changes in acetyl-CoA levels can alter H3K27ac modification, triggering the transcription of FOXM1 and nuclear translocation of β-catenin involved in the progression of glioblastoma multiforme [55]. Acetyl-CoA, a key substrate for histone acetylation, is involved in a range of biological functions, including energy metabolism, fatty acid metabolism, and cholesterol synthesis [43]. When cytoplasmic citrate (which can cross the nuclear membrane to produce acetyl-CoA via ACL is reduced due to production inhibition or diversion towards lipid synthesis, a nuclear source of acetyl-CoA becomes critical. Nuclear PDC generates acetyl-CoA necessary for histone acetylation, establishing a connection between metabolism and epigenetic regulation [16]. We demonstrated that PDHA1 was abundant and functional in the nucleus of AnoR PCa cells. Nuclear PDHA1 could produce acetyl coenzyme A for histone acetylation, providing an experimental basis for further studies of epigenetic and PCa metastasis.

PPARA, an intracellular fatty acid sensor, modulates lipid remodeling by transactivating genes involved in lipid metabolism [35]. Owing to its role in metabolic modulation and its druggable nature, PPAR agonists have been developed and utilized to treat metabolic disorders, particularly dyslipidemia and type 2 diabetes mellitus (T2DM). For instance, fibrates, which are selective

`

PPARα agonists, are commonly prescribed in combination with statins for treating atherosclerotic hyperlipidemia and hypertriglyceridemia [56]. GW6471, a competitive PPARA antagonist, at nanomolar concentrations, is widely used pharmacologically as an agent for blocking PPARA activation. Its antitumor effects have been investigated in a renal cancer cell model, where GW6471 had the ability to induce apoptosis and cell cycle arrest in the G0/G1 phase, and was associated with a significant reduction in cyclin D1, CDK4, and c-Myc protein expression [36]. Evidence showed that PPARA was also intimately associated with ferroptosis [57]. In this study, we found that PDHA1 was unable to significantly impact AIFM2 expression directly through histone acetylation but indirectly affected AIFM2 expression by enriching H3K9Ac in the PPARA promoter region to influence PPARA transcriptional activation. Through the dual-luciferase reporter assay, we found that PPARA positively regulated AIFM2 and PPARA overexpression enhanced the PDHA1 overexpression-induced elevation of AIFM2 relative reporter gene activity and protein levels. We further confirm that PDHA1 upregulates AIFM2 expression through PPARA.

Because PDHA1 is essential for normal metabolism, systemic inhibition may induce on-target toxicity. Tumor-selective approaches provide feasible solutions. Nanoparticle-based carriers can enhance tumor accumulation of PDHA1 inhibitors via the enhanced permeability and retention (EPR) effect or active targeting using antibodies, peptides, or glycan ligands. Stimuli-responsive nanocarriers, designed to release drugs in acidic, hypoxic, or enzyme-rich tumor environments, further improve selectivity [58]. Antibody–drug conjugates (ADCs) offer another level of precision by linking PDHA1 inhibitors to tumor-specific antibodies, thereby minimizing exposure of normal tissues [59]. For localized tumors, regional delivery strategies can also reduce systemic effects [60]. Together, these strategies highlight viable avenues to reduce toxicity while preserving the therapeutic potential of PDHA1-targeted therapies.

CONCLUSION

We demonstrated that PDHA1 expression was upregulated， and it was markedly translocated to the nucleus in AnoR PCa cells, causing an increase in H3K9Ac levels and enrichment in the PPARA promoter region, leading to PPARA transcriptional activation, which impacted the expression of

`

AIFM2 and might inhibit ferroptosis to promote prostate cancer metastasis. These insights may guide future therapeutic strategies targeting PDHA1-mediated ferroptosis suppression in metastatic prostate cancer

MATERIALS AND METHODS

1. Reagents

Ferrostatin-1 (S7243) was procured from Selleck Chemical (Shanghai, China). Z-VAD-FMK (HY-16658B), Erastin (HY-15763), Disulfiram (HY-B0240) and Necrostatin-2 (HY-14622) were purchased from MedChemExpress (Shanghai, China).

2. Cell culture and establishment of the anoikis resistance cell line

Human prostate cancer cell lines PC-3 and 22Rv1 were obtained from the Cell Bank of the Chinese Academy of Sciences (Shanghai, China). All cell lines were cultured in Roswell Park Memorial Institute (RPMI) 1640 medium (Hyclone, USA) supplemented with 10% fetal bovine serum (FBS) (Biological Industries, Israel) and incubated at 37 °C in a 5% CO2 environment. The AnoR cell model was constructed by using a method described in the previous study [21]. Each cell line was verified within six months prior to use using short tandem repeat profiling and was confirmed to be free of Mycoplasma contamination.

3. Human samples

Forty male prostate cancer tissue samples were obtained from the Department of Urology of Union Hospital, affiliated with Tongji Medical College. Informed consent was obtained from all participants. The study procedures adhered to the principles of the Declaration of Helsinki, and the research protocol received approval from the Research Ethics Committees of Union Hospital, Tongji Medical College, Huazhong University of Science and Technology, China.

4. Cell viability assay

Cell viability was assessed using the Cell Counting Kit-8 (CCK-8) assay (Dojindo Laboratories, Japan). Cell suspensions were prepared in complete medium， and 5000 cells were inoculated into each well of a 96-well plate and incubated for 24 hours. After the treatment, the CCK-8 working solution was prepared and incubated at 37°C in the dark for 1 hour. The optical density at 450 nm absorbance of each well was measured using a microplate reader (Tecan, Mannedorf, Switzerland).

5. Pyruvate dehydrogenase (PDH) activity assay

`

PDH activity was measured using the PDH Assay Kit (Solarbio, China) following the manufacturer's instructions.

6. Quantitative real-time PCR (qRT-PCR)

RNA from the cells was isolated with Trizol reagent (Invitrogen, USA). cDNA was generated from this RNA using the PrimeScript RT Reagent Kit (Takara, Japan). Quantitative real-time PCR (qRT-PCR) was carried out on a StepOnePlus™ Real-Time PCR System (Applied Biosystems, USA) utilizing the ChamQ SYBR qPCR Master Mix (Vazyme, China). 2-ΔΔCT method was employed for data processing, with ACTB (β-actin) serving as internal control. The primers used for mRNA expression are shown in Supplemental file 1.

7. Western blot

Cellular proteins were extracted using RIPA lysis buffer (Servicebio, China), and their concentration was determined with a BCA protein assay kit (Beyotime, China). The protein samples were then mixed with loading buffer (ThermoFisher Scientific, USA) and stored at -20°C. Electrophoresis was carried out using the sodium dodecyl sulfate-polyacrylamide gel electrophoresis and then the sample was transferred onto the polyvinylidene fluoride (PVDF) membrane (Millipore). Next, the membranes were blocked with 5% skim milk for 1-2 hours, followed by three 10-minute washes in Tris-buffered saline with Tween-20 (TBST) at room temperature. Afterward, they were incubated overnight at 4°C with the specific primary antibodies, followed by a 1 hour incubation with a horseradish peroxidase (HRP)-conjugated secondary antibody at room temperature. The protein bands were visualized using an Enhanced Chemiluminescence (ECL) Substrate Kit (Millipore). The following antibodies were used: HRP-conjugated Affinipure Goat anti-mouse antibody (SA00001-1, Proteintech), HRP-conjugated Affinipure Goat anti-rabbit antibody (SA00001-2, Proteintech), Anti-PDHA1(A13687, ABclonal), Anti-PPARA (A24835, ABclonal), Anti-AIFM2 (A22278, ABclonal), Anti-ACSL4 (A20414, ABclonal), Anti-SLC3A2 (A3658, ABclonal), Anti-SLC7A11 (A2413, ABclonal), Anti-GPX4 (A11243, ABclonal), Anti-H3K9Ac (A7255, ABclonal), Anti-GAPDH (10494-1-AP, Proteintech), Anti-Lamin B1 (66095-1-Ig, Proteintech), Anti-α Tubulin (11224-1-AP, Proteintech), Anti-DHODH (67977-1-Ig,

`

Proteintech)

8. Cell migration and invasion assays

The invasive and migratory potential of the cells was assessed using polycarbonate membrane with 8-μm pores inserted into 24-well Transwell plates (Corning, USA). For the migration assay, cells were first starved in serum-free medium for 18 hours. Then 4×10^4 cells, added to 200 μl of serum-free medium, were seeded into the upper chamber of transwell plates and 750 μl of complete medium was added to the lower chamber. The sample was cultured for 48 hours, and then non-migratory cells on the upper chamber of the transwell membrane were removed with a cotton swab. The migratory cells on the lower surface of the membrane were fixed with 4% paraformaldehyde for 15 minutes, stained with 0.1% crystal violet for 30 minutes at room temperature and washed three times with phosphate-buffered saline (PBS). The invasion experiments followed the same procedure as the migration assay, with the exception that 50 μl of Matrigel matrix (BD Biosciences, China) was applied to each upper chamber. Finally, three areas were randomly selected for cell counting under an inverted phase contrast microscope (Olympus, Japan).

9. Immunohistochemistry (IHC)

Samples were paraffinized, rehydrated, blocked with 3% H_2O_2 and then incubated with normal goat serum (Vector Laboratories, Burlingame, CA, USA). After overnight incubation at 4°C with primary antibodies Anti-PDHA1 (A13687, ABclonal) and Anti-AIFM2 (A22278, ABclonal), the sections were washed with PBS and incubated with biotinylated secondary antibodies (Vector Laboratories). Subsequently, the average optical density was calculated to assess immunoreactivity by combining the percentage and intensity of positively stained PCa cells.

10. Measurement of intracellular Fe^{2+}

Intracellular Fe^{2+} levels were measured using the FeRhoNox™-1 fluorescent probe (GORYO Chemical, Japan). Cells were cultured on dishes for 24 hours and then washed three times with PBS. The 5 μM concentration of the FeRhoNox™-1 probe was applied, and the cells were incubated for 1 hour, shielded from light. After three additional PBS washes, the nuclei were stained with DAPI for 15 minutes. The cells were then analyzed using a Nikon A1Si laser scanning confocal microscope (Nikon Instruments, Japan).

`

11. Malondialdehyde (MDA) detection

The intracellular MDA level was determined by using the MDA detection kit (A003-4-1, Nanjing Jiancheng Bioengineering Institute, China). Briefly, MDA in peroxidized lipid degradation products could condense with thiobarbituric acid (TBA) to form a red product at 95 °C for 40 minutes Absorbance was measured at 530 nm. MDA was expressed as nmol/mg (cell protein).

12. Intracellular ROS production assays

Intracellular ROS levels were analyzed by using a Reactive Oxygen Assay Kit (Beyotime, S0033, China) according to the manufacturer's instructions. Cells were seeded into 6-well plates and diluted DCFH-DA (a fluorescent probe sensitive to oxidation) was added the next day, and the cells were incubated at 37 °C for 20 minutes. After washing with serum-free medium three times, cells were digested with trypsin. The cells were then collected by centrifugation, and the resulting cells were resuspended in PBS. Reactive oxygen species (ROS) levels were subsequently measured using a flow cytometer (Beckman Coulter, USA).

13. Transmission electron microscopy

Following treatment, cells were fixed in 2.5% glutaraldehyde at 4°C for 2 hours, and transmission electron microscopy was performed by Servicebio (Wuhan, China).

14. Plasmid transfection

The plasmids with PDHA1 overexpression and knockdown, PPARA overexpression and knockdown, the overexpression lentivirus of nuclear localization signal fused PDHA1 (NLS-PDHA1), Renilla luciferase TK and NLS-PDHA1-mut were purchased from GeneChem (Shanghai, China). AIFM2-overexpressing plasmid was bought from Vigene Biosciences (Shandong, China). Firefly luciferase (FLuc) AIFM2-promoter wild type (wt), Fluc AIFM2 promoter mutant type and mutant type 1/2/3/4 were constructed by and purchased from General Biol (Anhui, China).

15. Immunofluorescence staining

Cells were inoculated in confocal dishes for 16 h. Subsequently, cells were fixed with 4% paraformaldehyde on ice for 20 minutes, permeabilized with 0.3% Triton X-100 for 5 minutes and blocked with 3% BSA for 1 hour at room temperature. Then, cells were incubated with primary antibodies overnight at 4°C. On the following day, cells were incubated for 1 hour with

`

fluorescently labeled secondary antibodies, and nuclei were stained with DAPI for 15 minutes. For mitochondrial immunofluorescence, cells were incubated with 100 nM MitoTracker® Red CMXRos (40741ES50, YEASEN, China) for 30 minutes in the dark prior to fixation. Fluorescence images were then captured using a Nikon A1Si laser scanning confocal microscope (Nikon Instruments, Japan). For specific molecular labeling, Anti-PDHA1 (A13687, ABclonal) and CoraLite 488-conjugated Goat Anti-Rabbit IgG (H + L) (SA00013-2, Proteintech) were used.

16. Chromatin immunoprecipitation (ChIP)

The ChIP assay kit (P2078, Beyotime, China) was used by following the manufacturer's instructions. Briefly, cells were mixed at 37°C with an appropriate amount of formaldehyde to a final concentration of 1%, and the reaction was terminated by adding 0.125 M glycine for 10 minutes at room temperature. Cells were washed twice with pre-cooled PBS containing 1 mM PMSF, harvested into SDS lysis buffer of the ChIP assay kit, then lysed on ice prior to sonication, and finally, incubated overnight with specific primary antibodies at 4°C. The DNA fragments were then purified using a DNA purification kit (D0033, Beyotime, China). Primers used for ChIP-qPCR were in Supplemental file 1.

17. Dual-luciferase reporter assay

Cells were uniformly seeded into 6-well culture plates and transfected with the PPARA overexpression plasmid, pGL3-basic luciferase reporter plasmids containing AIFM2 promoter and Renilla luciferase TK plasmid to assess the transcriptional regulation of AIFM2 by PPARA. To identify specific binding sites between PPARA and AIFM2, cells were transfected with wild-type or mutant plasmids containing the AIFM2 promoter along with the PPARA overexpression plasmid. Cells were then cultured for 48 hours. Luciferase activities were measured according to the manufacturer's instructions on the Dual- Luciferase Reporter Assay System (RG027, Beyotime, China).

18. Nuclear and cytosolic protein extraction

Nuclear and cytoplasmic fractions were isolated using the Nuclear and Cytoplasmic Protein Extraction Kit (P0027, Beyotime, China). Western blot analysis was then conducted on the extracted proteins, with Lamin B1 and α tubulin serving as internal controls for the nuclear and cytoplasmic fractions, respectively.

`

19. Mitochondrial Membrane Potential (MMP) Assays

Mitochondrial Membrane Potential was detected using the Mitochondrial membrane potential assay kit with JC-1 (C2006, Beyotime, China) according to the manufacturer's instructions. In normal cells with high MMP, JC-1 spontaneously forms J-aggregates in mitochondria and emits red fluorescence. However, in abnormal cells, MMP decreases, and JC-1 is released from mitochondria and exists as a monomer, emitting green fluorescence. Images were taken under an inverted phase contrast microscope (Olympus, Japan).

20. Wound healing assay

The cells were cultured in six-well plates until confluence. A pipette tip was used to draw a line across the layer of cells to simulate the wound. The wound was photographed after 0 and 24 h of serum-free 1640 medium incubation. Floating cells and shattering pieces were removed by PBS rinsing before photographing. All experiments were repeated three times, and the results were analyzed by ImageJ.

21. Tumor xenograft assay

The 4-week-old male athymic BALB/c nude mice were purchased from Beijing HFK Bioscience Co. Ltd. All animal experiments were approved by the Ethics Committee for Animal Experiments at Huazhong University of Science and Technology, China. During the study, mice were randomly assigned to experimental groups (five mice per group). To establish a lung metastasis model, we injected stably transfected AnoR PC-3 cells (2×10^6) into the tail vein of each mouse. The mice were monitored daily after injection and allowed to survive until natural death. Those that did not die spontaneously within eight weeks were humanely sacrificed at that time. Lungs were then collected for fluorescence imaging using the FX PRO Imaging System (Bruker Corporation, USA) under standardized exposure settings (570 nm).

22. Co-immunoprecipitation (Co-IP) assay

After treatment, the cells were collected by centrifugation in prechilled PBS and lysed using NP-40 buffer supplemented with protease inhibitors. Approximately 5% of the total lysate was retained as an input control, and the remaining portion was incubated with protein A/G beads at room temperature for 2 hours to reduce nonspecific binding. The resulting mixture was evenly distributed into two microcentrifuge tubes and incubated overnight at 4 °C with either 5 μg of FLAG antibody or an IgG isotype control. The following day, fresh protein A/G beads were added, and the samples were rotated for an additional 3 hours at 4 °C. After thorough washing,

`

sample buffer was added, and the bound proteins were subjected to western blot analysis. Co-immunoblotting was performed using the following antibodies: Rabbit IgG control (AC005, Abclonal) and anti-DDDDK-tag antibody (AE005, Abclonal).

23. Lipid reactive oxygen species (ROS)

The C11-BODIPY 581/591 probe (S0043S, Beyotime, China) was employed to measure the levels of lipid reactive oxygen species (ROS), following the instructions provided in the manual.

24.Statistical analysis

Data were analyzed using GraphPad Prism 8.0 (La Jolla, CA, USA) software and expressed as mean ± standard deviation (SD). A two-tailed Student's t-test was used to compare differences between two groups, while analysis of variance (ANOVA) was employed for comparisons involving multiple groups. Kaplan-Meier analysis was performed to evaluate survival data, with the log-rank test used to compare survival differences. All in vitro experiments were repeated 3 times. $P < 0.05$ was considered statistically significant (* $P < 0.05$, ** $P < 0.01$, *** $P < 0.001$, **** $P < 0.0001$).、

DATA AVAILABILITY

The data that support the findings of this study are available from the corresponding author upon reasonable request

REFERENCES

1. Bray F, Laversanne M, Sung H, Ferlay J, Siegel RL, Soerjomataram I, et al. Global cancer statistics 2022: GLOBOCAN estimates of incidence and mortality worldwide for 36 cancers in 185 countries. CA Cancer J Clin. 2024;74(3):229-63.

2. Smith MR, Mehra M, Nair S, Lawson J, Small EJ. Relationship Between Metastasis-free Survival and Overall Survival in Patients With Nonmetastatic Castration-resistant Prostate Cancer. Clin Genitourin Cancer. 2020;18(2):e180-e9.

3. Sandhu S, Moore CM, Chiong E, Beltran H, Bristow RG, Williams SG. Prostate cancer. Lancet. 2021;398(10305):1075-90.

4. Massague J, Obenauf AC. Metastatic colonization by circulating tumour cells. Nature. 2016;529(7586):298-306.

`

5. Sun J, Li J, Pantopoulos K, Liu Y, He Y, Kang W, et al. The clustering status of detached gastric cancer cells inhibits anoikis-induced ferroptosis to promote metastatic colonization. Cancer Cell Int. 2024;24(1):77.

6. Nalla LV, Khairnar A. Empagliflozin drives ferroptosis in anoikis-resistant cells by activating miR-128-3p dependent pathway and inhibiting CD98hc in breast cancer. Free Radic Biol Med. 2024;220:288-300.

7. Galluzzi L, Vitale I, Aaronson SA, Abrams JM, Adam D, Agostinis P, et al. Molecular mechanisms of cell death: recommendations of the Nomenclature Committee on Cell Death 2018. Cell Death Differ. 2018;25(3):486-541.

8. Stockwell BR. Ferroptosis turns 10: Emerging mechanisms, physiological functions, and therapeutic applications. Cell. 2022;185(14):2401-21.

9. Wang Y, Wu X, Ren Z, Li Y, Zou W, Chen J, et al. Overcoming cancer chemotherapy resistance by the induction of ferroptosis. Drug Resist Updat. 2023;66:100916.

10. Dixon SJ, Lemberg KM, Lamprecht MR, Skouta R, Zaitsev EM, Gleason CE, et al. Ferroptosis: an iron-dependent form of nonapoptotic cell death. Cell. 2012;149(5):1060-72.

11. Wang N, Ma T, Yu B. Targeting epigenetic regulators to overcome drug resistance in cancers. Signal Transduct Target Ther. 2023;8(1):69.

12. Zhu Q, Belden WJ. Molecular Regulation of Circadian Chromatin. J Mol Biol. 2020;432(12):3466-82.

13. Wang C, Zeng J, Li LJ, Xue M, He SL. Cdc25A inhibits autophagy-mediated ferroptosis by upregulating ErbB2 through PKM2 dephosphorylation in cervical cancer cells. Cell Death Dis. 2021;12(11):1055.

14. Sutendra G, Kinnaird A, Dromparis P, Paulin R, Stenson TH, Haromy A, et al. A nuclear pyruvate dehydrogenase complex is important for the generation of acetyl-CoA and histone acetylation. Cell. 2014;158(1):84-97.

15. He W, Li Q, Li X. Acetyl-CoA regulates lipid metabolism and histone acetylation modification in cancer. Biochim Biophys Acta Rev Cancer. 2023;1878(1):188837.

16. Whitley MJ, Arjunan P, Nemeria NS, Korotchkina LG, Park YH, Patel MS, et al. Pyruvate dehydrogenase complex deficiency is linked to regulatory loop disorder in the alphaV138M variant of human pyruvate dehydrogenase. J Biol Chem. 2018;293(34):13204-13.

17. Park S, Jeon JH, Min BK, Ha CM, Thoudam T, Park BY, et al. Role of the Pyruvate Dehydrogenase

`

Complex in Metabolic Remodeling: Differential Pyruvate Dehydrogenase Complex Functions in Metabolism. Diabetes Metab J. 2018;42(4):270-81.

18. Fan J, Shan C, Kang HB, Elf S, Xie J, Tucker M, et al. Tyr phosphorylation of PDP1 toggles recruitment between ACAT1 and SIRT3 to regulate the pyruvate dehydrogenase complex. Mol Cell. 2014;53(4):534-48.

19. Dan L, Wang C, Ma P, Yu Q, Gu M, Dong L, et al. PGC1alpha promotes cholangiocarcinoma metastasis by upregulating PDHA1 and MPC1 expression to reverse the Warburg effect. Cell Death Dis. 2018;9(5):466.

20. Chen J, Li ZY, Zheng G, Cao L, Guo YM, Lian Q, et al. RNF4 mediated degradation of PDHA1 promotes colorectal cancer metabolism and metastasis. NPJ Precis Oncol. 2024;8(1):258.

21. Liu B, Li X, Wang D, Yu Y, Lu D, Chen L, et al. CEMIP promotes extracellular matrix-detached prostate cancer cell survival by inhibiting ferroptosis. Cancer Sci. 2022;113(6):2056-70.

22. Chen J, Guccini I, Di Mitri D, Brina D, Revandkar A, Sarti M, et al. Compartmentalized activities of the pyruvate dehydrogenase complex sustain lipogenesis in prostate cancer. Nat Genet. 2018;50(2):219-28.

23. Zhang P, Song Y, Sun Y, Li X, Chen L, Yang L, et al. AMPK/GSK3beta/beta-catenin cascade-triggered overexpression of CEMIP promotes migration and invasion in anoikis-resistant prostate cancer cells by enhancing metabolic reprogramming. FASEB J. 2018;32(7):3924-35.

24. Park E, Chung SW. ROS-mediated autophagy increases intracellular iron levels and ferroptosis by ferritin and transferrin receptor regulation. Cell Death Dis. 2019;10(11):822.

25. Li D, Wang Y, Dong C, Chen T, Dong A, Ren J, et al. CST1 inhibits ferroptosis and promotes gastric cancer metastasis by regulating GPX4 protein stability via OTUB1. Oncogene. 2023;42(2):83-98.

26. Zhao Y, Liu Z, Liu G, Zhang Y, Liu S, Gan D, et al. Neutrophils resist ferroptosis and promote breast cancer metastasis through aconitate decarboxylase 1. Cell Metab. 2023;35(10):1688-703 e10.

27. Xiong H, Zhai Y, Meng Y, Wu Z, Qiu A, Cai Y, et al. Acidosis activates breast cancer ferroptosis through ZFAND5/SLC3A2 signaling axis and elicits M1 macrophage polarization. Cancer Lett. 2024;587:216732.

28. Liang D, Feng Y, Zandkarimi F, Wang H, Zhang Z, Kim J, et al. Ferroptosis surveillance independent of GPX4 and differentially regulated by sex hormones. Cell. 2023;186(13):2748-64 e22.

29. Lang X, Green MD, Wang W, Yu J, Choi JE, Jiang L, et al. Radiotherapy and Immunotherapy Promote Tumoral Lipid Oxidation and Ferroptosis via Synergistic Repression of SLC7A11. Cancer Discov.

`

2019;9(12):1673-85.

30. Liao P, Wang W, Wang W, Kryczek I, Li X, Bian Y, et al. CD8(+) T cells and fatty acids orchestrate tumor ferroptosis and immunity via ACSL4. Cancer Cell. 2022;40(4):365-78 e6.

31. Mao C, Liu X, Zhang Y, Lei G, Yan Y, Lee H, et al. DHODH-mediated ferroptosis defence is a targetable vulnerability in cancer. Nature. 2021;593(7860):586-90.

32. Bersuker K, Hendricks JM, Li Z, Magtanong L, Ford B, Tang PH, et al. The CoQ oxidoreductase FSP1 acts parallel to GPX4 to inhibit ferroptosis. Nature. 2019;575(7784):688-92.

33. Aguzzi A, Altmeyer M. Phase Separation: Linking Cellular Compartmentalization to Disease. Trends Cell Biol. 2016;26(7):547-58.

34. Bates SE, Longo DL. Epigenetic Therapies for Cancer. New England Journal of Medicine. 2020;383(7):650-63.

35. Cheng HS, Tan WR, Low ZS, Marvalim C, Lee JYH, Tan NS. Exploration and Development of PPAR Modulators in Health and Disease: An Update of Clinical Evidence. International Journal of Molecular Sciences. 2019;20(20).

36. Lin Z, Liu J, Long F, Kang R, Kroemer G, Tang D, et al. The lipid flippase SLC47A1 blocks metabolic vulnerability to ferroptosis. Nature Communications. 2022;13(1).

37. Strilic B, Offermanns S. Intravascular Survival and Extravasation of Tumor Cells. Cancer Cell. 2017;32(3):282-93.

38. Jin K, Li T, van Dam H, Zhou F, Zhang L. Molecular insights into tumour metastasis: tracing the dominant events. The Journal of Pathology. 2017;241(5):567-77.

39. Wang Y, Cheng S, Fleishman JS, Chen J, Tang H, Chen Z-S, et al. Targeting anoikis resistance as a strategy for cancer therapy. Drug Resistance Updates. 2024;75.

40. Wang Y, Fleishman JS, Wang J, Chen J, Zhao L, Ding M. Pharmacologically inducing anoikis offers novel therapeutic opportunities in hepatocellular carcinoma. Biomedicine & Pharmacotherapy. 2024;176.

41. Wang H, Sun J, Sun H, Wang Y, Lin B, Wu L, et al. The OGT–c-Myc–PDK2 axis rewires the TCA cycle and promotes colorectal tumor growth. Cell Death & Differentiation. 2024;31(9):1157-69.

42. Cai Z, Li C-F, Han F, Liu C, Zhang A, Hsu C-C, et al. Phosphorylation of PDHA by AMPK Drives TCA

`

Cycle to Promote Cancer Metastasis. Molecular Cell. 2020;80(2):263-78.e7.

43. Han A, Chua V, Baqai U, Purwin TJ, Bechtel N, Hunter E, et al. Pyruvate dehydrogenase inactivation causes glycolytic phenotype in BAP1 mutant uveal melanoma. Oncogene. 2022;41(8):1129-39.

44. Commander R, Wei C, Sharma A, Mouw JK, Burton LJ, Summerbell E, et al. Subpopulation targeting of pyruvate dehydrogenase and GLUT1 decouples metabolic heterogeneity during collective cancer cell invasion. Nature Communications. 2020;11(1).

45. Jin L, Chun J, Pan C, Kumar A, Zhang G, Ha Y, et al. The PLAG1-GDH1 Axis Promotes Anoikis Resistance and Tumor Metastasis through CamKK2-AMPK Signaling in LKB1-Deficient Lung Cancer. Molecular Cell. 2018;69(1):87-99.e7.

46. Taddei ML, Giannoni E, Fiaschi T, Chiarugi P. Anoikis: an emerging hallmark in health and diseases. The Journal of Pathology. 2011;226(2):380-93.

47. Lu J, Tan M, Cai Q. The Warburg effect in tumor progression: Mitochondrial oxidative metabolism as an anti-metastasis mechanism. Cancer Letters. 2015;356(2):156-64.

48. Chi W, Kang N, Sheng L, Liu S, Tao L, Cao X, et al. MCT1-governed pyruvate metabolism is essential for antibody class-switch recombination through H3K27 acetylation. Nature Communications. 2024;15(1).

49. Schwab A, Rao Z, Zhang J, Gollowitzer A, Siebenkas K, Bindel N, et al. Zeb1 mediates EMT/plasticity-associated ferroptosis sensitivity in cancer cells by regulating lipogenic enzyme expression and phospholipid composition. Nat Cell Biol. 2024;26(9):1470-81.

50. Dai E, Zhang W, Cong D, Kang R, Wang J, Tang D. AIFM2 blocks ferroptosis independent of ubiquinol metabolism. Biochemical and Biophysical Research Communications. 2020;523(4):966-71.

51. Guo S, Li F, Liang Y, Zheng Y, Mo Y, Zhao D, et al. AIFM2 promotes hepatocellular carcinoma metastasis by enhancing mitochondrial biogenesis through activation of SIRT1/PGC-1α signaling. Oncogenesis. 2023;12(1).

52. Chen Y, Zhou Y, Yin H. Recent advances in biosensor for histone acetyltransferase detection. Biosensors and Bioelectronics. 2021;175.

53. Shahbazian MD, Grunstein M. Functions of Site-Specific Histone Acetylation and Deacetylation. Annual Review of Biochemistry. 2007;76(1):75-100.

`

54. Cui X, Yun X, Sun M, Li R, Lyu X, Lao Y, et al. HMGCL-induced β-hydroxybutyrate production attenuates hepatocellular carcinoma via DPP4-mediated ferroptosis susceptibility. Hepatology International. 2022;17(2):377-92.

55. Sun Y, Mu G, Zhang X, Wu Y, Wang S, Wang X, et al. Metabolic modulation of histone acetylation mediated by HMGCL activates the FOXM1/β-catenin pathway in glioblastoma. Neuro-Oncology. 2024;26(4):653-69.

56. Grundy SM, Stone NJ, Bailey AL, Beam C, Birtcher KK, Blumenthal RS, et al. 2018 AHA/ACC/AACVPR/AAPA/ABC/ACPM/ADA/AGS/APhA/ASPC/NLA/PCNA Guideline on the Management of Blood Cholesterol: A Report of the American College of Cardiology/American Heart Association Task Force on Clinical Practice Guidelines. Circulation. 2019;139(25).

57. Kyprianou N, Abu Aboud O, Wettersten HI, Weiss RH. Inhibition of PPARα Induces Cell Cycle Arrest and Apoptosis, and Synergizes with Glycolysis Inhibition in Kidney Cancer Cells. PLoS ONE. 2013;8(8).

58. Mi P. Stimuli-responsive nanocarriers for drug delivery, tumor imaging, therapy and theranostics. Theranostics. 2020;10(10):4557-88.

59. Dumontet C, Reichert JM, Senter PD, Lambert JM, Beck A. Antibody-drug conjugates come of age in oncology. Nat Rev Drug Discov. 2023;22(8):641-61.

60. Janssen JC, van Dijk B, Hoeijmakers LL, Grunhagen DJ, Bramer WM, Verhoef C, et al. Local administration of immunotherapy for patients with skin cancer: A systematic review. Cancer Treat Rev. 2024;131:102848.

CRediT authorship contribution statement

YKC: Writing original-draft, Formal analysis, Data curation, Conceptuation. KC: Visualization, Formal analysis. YJJ: Visualization. CYL, QLH and JWC: methodology, Writing-review&editing. FL, JYC: Formal analysis. HRL Visualization, Supervision. LC: Investigation. YRS: funding acquisition, Project administration. All authors read and approved the final paper

Acknowledgements

This work was supported by the National Natural Science Foundation of China no.82103610 to YRS

Conflict of Interest

`

The authors declare no competing financial interests.

`

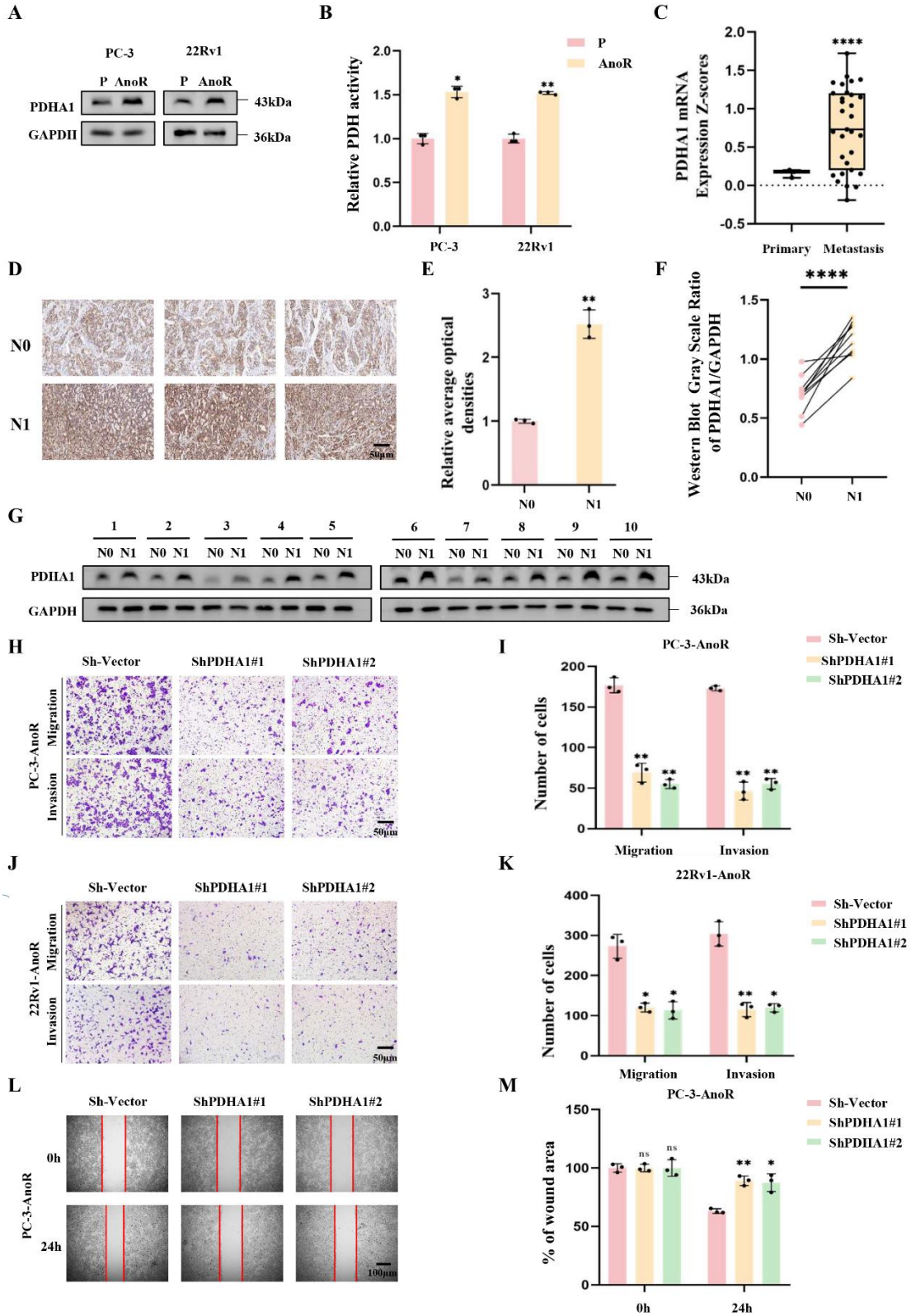

Fig. 1 PDHA1 is highly expressed in AnoR PCa cells and promotes tumor metastasis and survival

`

(**A**) Western blot analysis of PDHA1 expression in parental (P) and AnoR PCa cells. (**B)** Relative PDH activity in parental (P) and AnoR PCa cells. (**C**) mRNA expression Z-scores of PDHA1 in primary and metastatic prostate cancer. Samples in indicated comparison from the cBioPortal cohort. (D, E) Immunohistochemistry (IHC) of PDHA1 expression **(D)** and relative average optical densities **(E)** in PCa tissues with negative (N0) and positive for lymph node metastasis (N1). Scale bars, 50 μm. (F.G) Western blot of PDHA1 expression in PCa tissues with negative (N0) and positive (N1) for lymph node metastasis **(G)** with densitometric and statistical analysis **(F)**. **(H-K)** Transwell analysis of the migration and invasion of AnoR PCa cells with PDHA1 knockdown. Scale bars, 50 μm. **(L.M)** Scratch-wound healing assays assessing migration in AnoR PC-3 cells with or without PDHA1 knockdown. Scale bars, 100 μ m. Data are presented as representative images or as the mean ± SD of three independent experiments. * $P <$ 0.05, ** $P < 0.01$, ****$P < 0.0001$, ns, not significant.

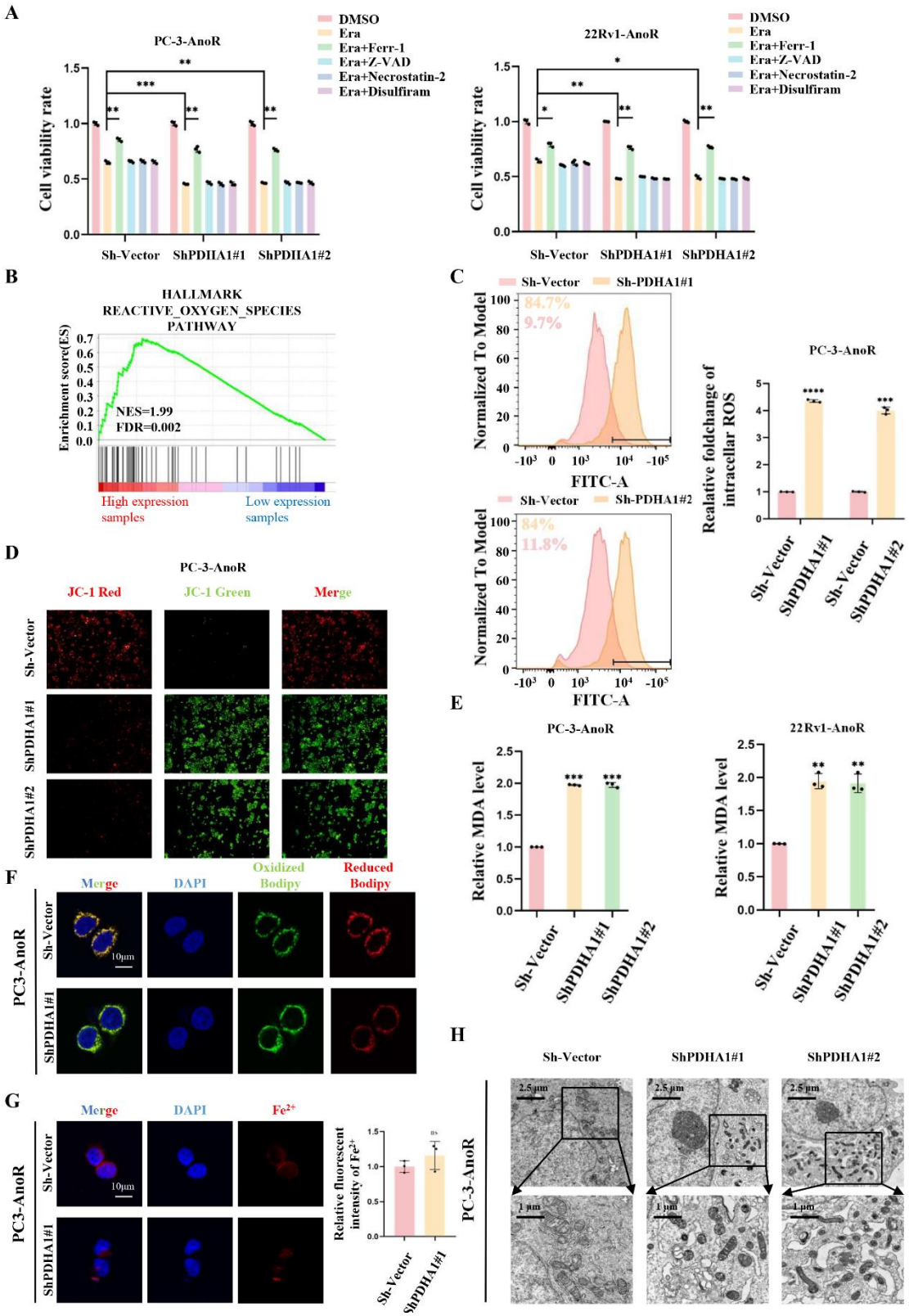

Fig. 2 PDHA1 promotes ferroptosis resistance in AnoR PCa cells

`

(**A**) Cell viability of AnoR PCa cells with PDHA1 knockdown after 24h treat with Erastin (Era, 5 μM), Erastin (Era, 5 μM) in combination with Ferrostatin-1 (Ferr-1, 5 μM), Z-VAD-FMK (Z-VAD, 20 μM), Necrostatin-2 (20 μM) and Disulfiram (20μM), respectively. (**B)** GSEA of PDHA1 high and low expression groups for reactive oxygen species (ROS)-related gene sets from the Hallmark database. (C) Intracellular ROS levels in PDHA1 knockdown AnoR PC-3 cells were detected by flow cytometry using DCFH-DA staining with corresponding quantitative bar graphs. (**D**) MMP assessed by JC-1 staining in AnoR PC-3 cells transfected with sh-vector, shPDHA1#1 and shPDHA1#2. (**E)** Content of MDA in PDHA1 knockdown AnoR PCa cells. (**F)** The levels of lipid ROS measured with C11-BODIPY 581/591 probe. Scale bars, 10 μm. (**G)** Confocal imaging of intracellular Fe^{2+} levels in AnoR PC-3 cells using a FeRhoNox™-1 fluorescent probe. Scale bars, 10 μm. (**H)** Mitochondrial morphological changes in PDHA1 knockdown AnoR PC-3 cells were observed by transmission electron microscopy. Scale bars, 2.5 μm and 1 μm, respectively. Data are presented. as representative images or as the mean ± SD of three independent experiments. $*P < 0.05$, $**P < 0.01$, $*** P < 0.001$, $****P < 0.0001$.

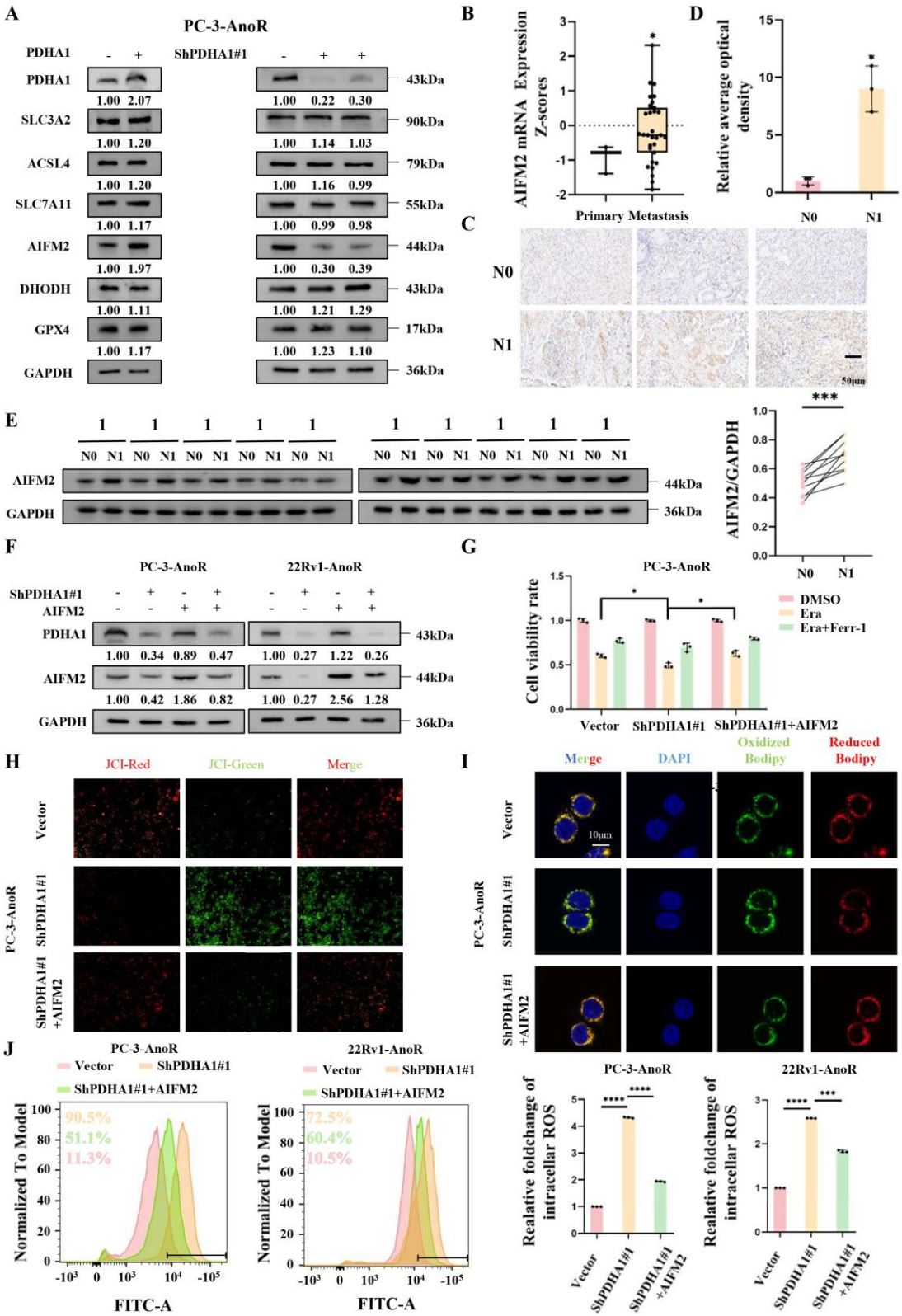

Fig. 3 PDHA1 inhibits ferroptosis in AnoR PCa cells by upregulating AIFM2

`

A. Western blot was performed to detect protein levels of ferroptosis-related genes in PDHA1 overexpression and knockdown AnoR PC-3 cells. **B**. The mRNA expression Z-scores of AIFM2 in primary and metastatic prostate cancer. Samples in indicated comparison from cBioPortal cohorts. (C-D) Immunohistochemical evaluation **(C)** and quantification of relative average optical densities **(D)** of AIFM2 expression in PCa tissues with negative (N0) and positive lymph-node metastasis (N1). Scale bars, 50 μm. (**E**) Western blot analysis of PDHA1 expression in PCa tissues with negative lymph-node metastasis (N0) and positive lymph-node metastasis (N1). (**F**) Western blot was performed to detect the reversal effect of AIFM2 overexpression following PDHA1 knockdown in AnoR PCa cell lines. (**G)** The cell viability of PDHA1 knockdown and AIFM2-overexpressing PCa cells after 24 h of Era (5 μM) and Era (5 μM) with Ferr-1 (5 μM) was detected by CCK-8 assay in AnoR PC-3 cells. (**H**)MMP in AnoR PC-3 cells was assessed by JC-1 staining. **(I)** The levels of lipid ROS measured with C11-BODIPY 581/591 probe. Scale bars, 10 μm. (**J**) Intracellular ROS in each group were detected by flow cytometry using DCFH-DA staining and the corresponding bar graph of active oxygen levels. Data are presented as representative images or as the mean ± SD of three independent experiments. $*P < 0.05$; $***P < 0.001$; $****P < 0.0001$.

`

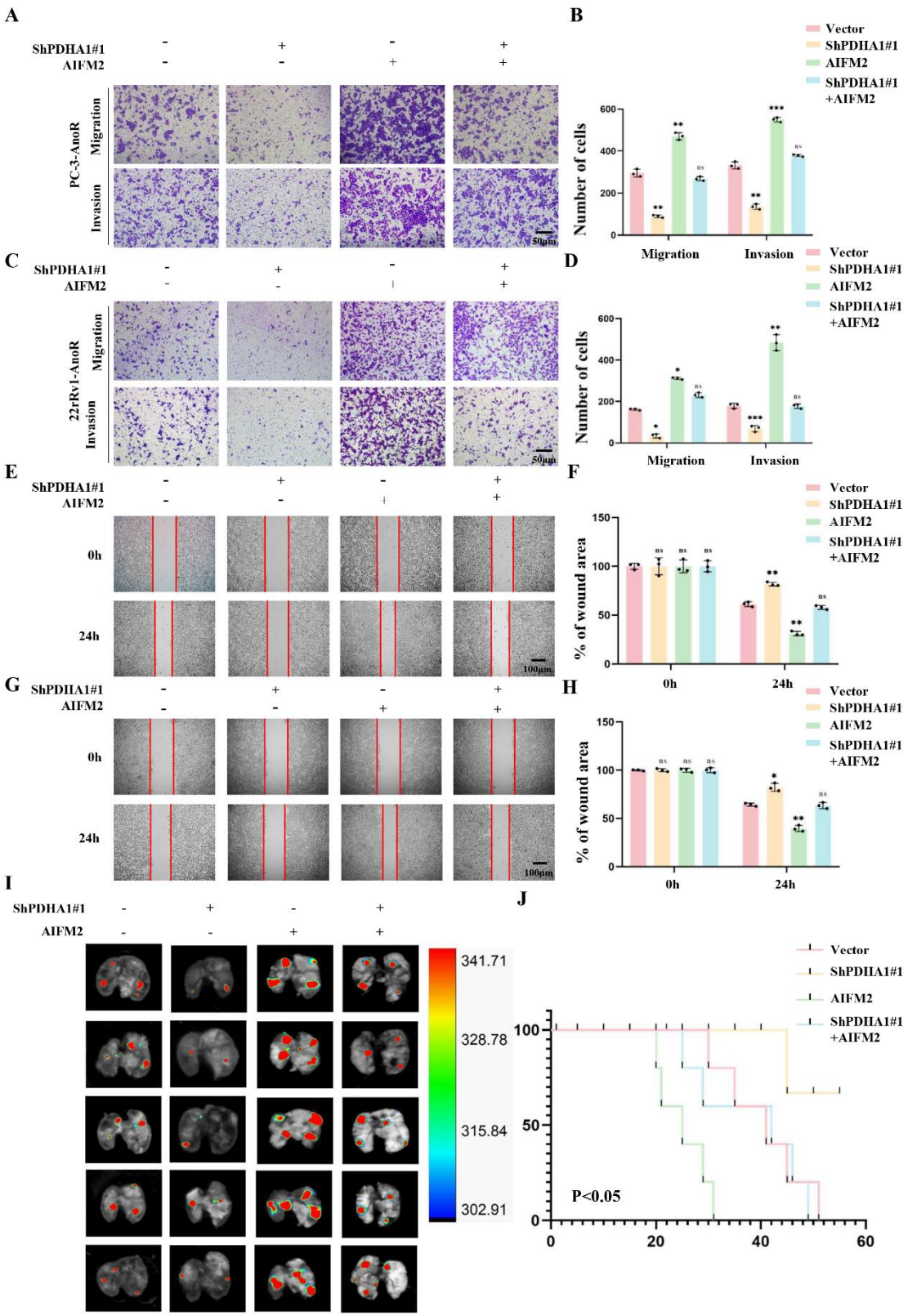

Fig. 4. AIFM2 rescues progression of PDHA1 knockdown AnoR PCa cells

`

(**A-B**) Transwell analysis of the migratory and invasive capacities of stably transfected AnoR PC-3 cells. Scale bars, 50 μm. (**C-D**) Transwell analysis of the migratory and invasive capacities of stably transfected AnoR 22Rv1 cells. Scale bars, 50 μm. (**E-F**) Wound healing assay of metastasis capacity of stably transfected AnoR PC-3 cells. Scale bars, 100 μm. (**G-H)** Wound healing assay of metastasis capacity of stably transfected AnoR 22Rv1 cells. Scale bars, 100 μm. (I-J) Representative bioluminescence images of metastatic lung colonization in nude mice injected with the corresponding cells via the tail vein (**I**) and Kaplan-Meier survival curves of metastasis assays in nude mice (**J**). Data are presented as representative images or as the mean ± SD of three independent experiments. *$P < 0.05$; **$P < 0.01$; ***$P < 0.001$; ns, not significant.

`

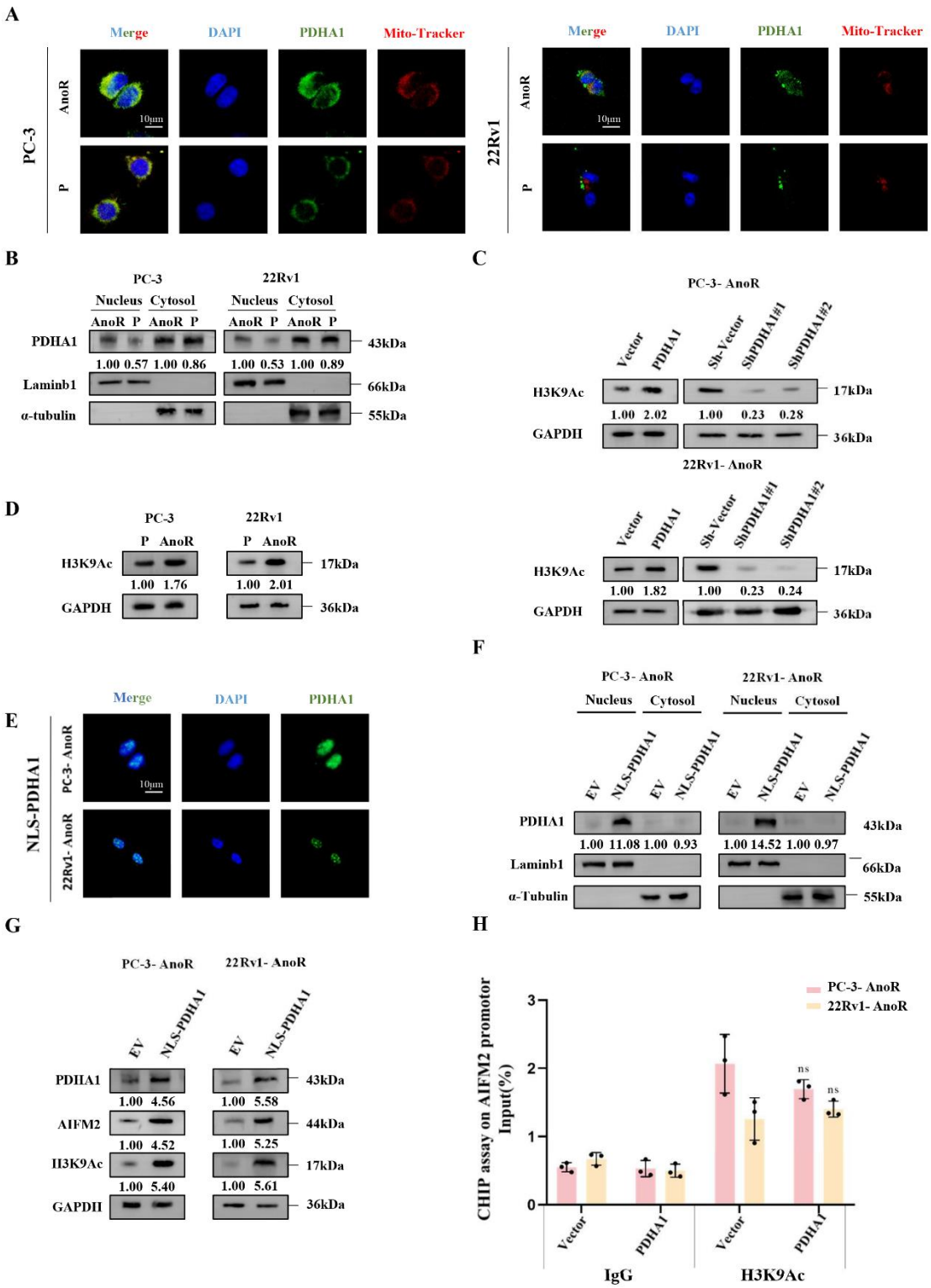

Fig. 5 PDHA1 promotes downstream gene expression by translocating into the nucleus to regulate

`

histone acetylation

(**A**) Representative confocal images of PDHA1 in AnoR and parental (P) cells (blue, DAPI; green, PDHA1; red, MitoTracker). Scale bars,10 μm. (**B**) Western blot of PDHA1 expression in the nuclear and cytoplasmic fractions of AnoR cells and parental (P) cells (**C)** Western blot for the detection of expression levels of H3K9Ac in PDHA1 overexpression and knockdown AnoR PC-3 and 22Rv1 cells. (**D**) Western blot of H3K9Ac expression in parental(P) and AnoR PCa cells. (**E**) Representative confocal images of shPDHA1 AnoR PCa cells infected with NLS-PDHA1 alone (blue, DAPI; green, PDHA1). Scale bars, 10 μm. (**F**) Western blot analysis of PDHA1 expression in the nuclear and cytoplasmic compartments of AnoR PCa cells with or without NLS-PDHA1 infection. (**G**) Western blot analysis of indicated proteins in shPDHA1 AnoR PC-3 and 22Rv1 cellsnfected with or without NLS-PDHA1 infection. (**H**) Chromatin immunoprecipitation of the binding of H3K9Ac at the promoter of AIFM2. Data are presented as representative images or as the mean ± SD of three independent experiments. ns, not significant.

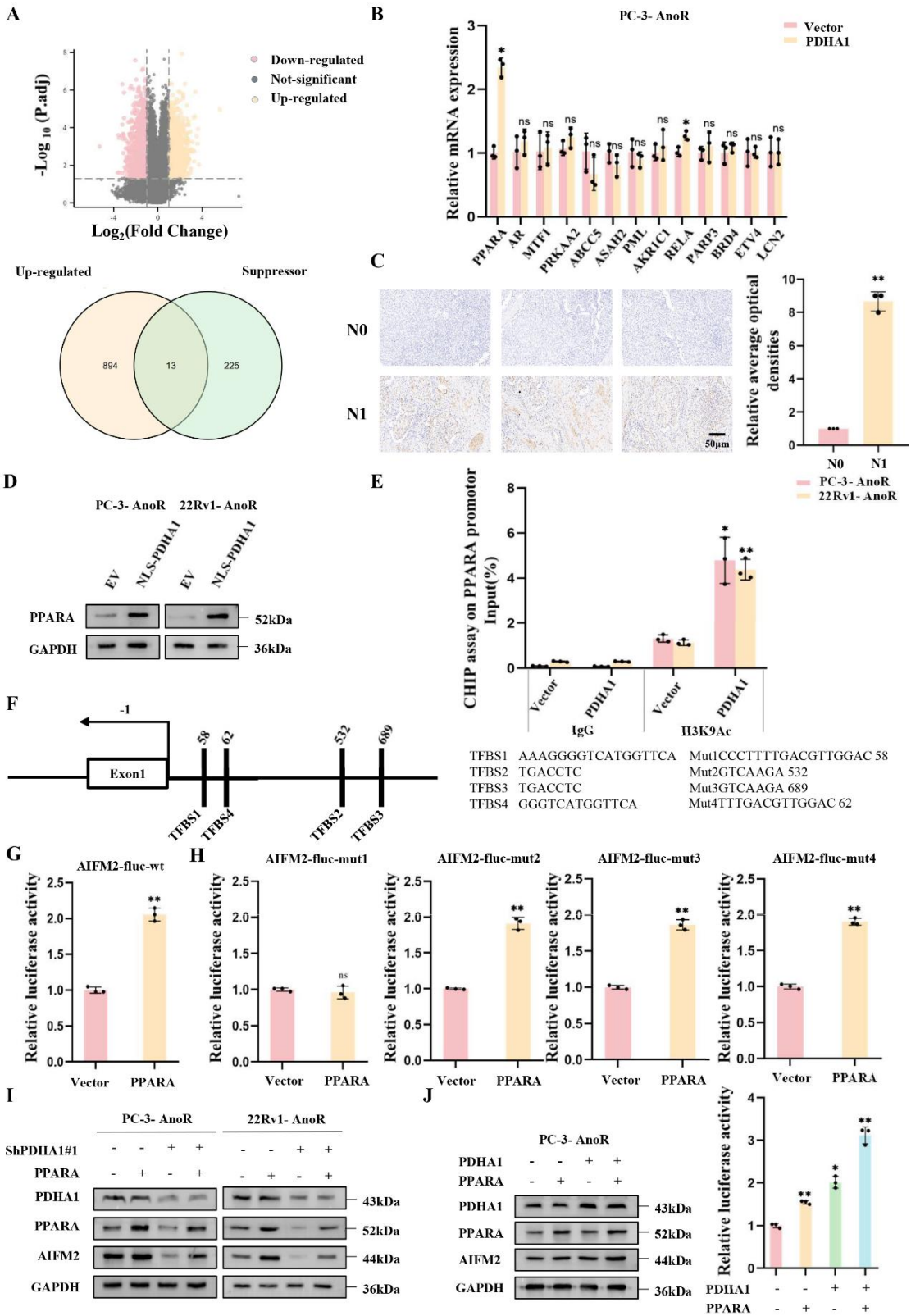

Fig. 6 PDHA1 upregulates AIFM2 expression by promoting transcriptional activation of PPARA

`

(**A**) Volcano plot of differentially expressed genes (DEGs) in the GSE100629 dataset. Venn diagram illustrating the overlap between upregulated genes in the GSE100629 dataset and ferroptosis-suppressing genes in the FerrDb V2 database. (**B**) qRT-PCR analysis of 13 genes that were upregulated in AnoR cells and shown to repress ferroptosis in AnoR PC-3 cells following PDHA1 overexpression. (**C**) Chromatin immunoprecipitation analysis showing H3K9Ac enrichment at the promoter region of PPARA. (**D**) Western blot analysis of PPARA expression in shPDHA1 AnoR PCa cells with or without NLS-PDHA1 infection. (**E**) Immunohistochemistry (IHC) of PDHA1 expression and relative average optical densities in PCa tissues with negative (N0) and positive for lymph node metastasis (N1). Scale bars, 50 μm. (**F**) Predicted transcription factor binding site maps showing four corresponding mutation sites within the PPARA and AIFM2 promoters. (**G**) Luciferase activity of wt AIFM2 promoter after transfection of PPARA-overexpressing plasmid in AnoR PC-3 cells. (**H**) Luciferase reporter assay showing the activity of the wt AIFM2 promoter after transfection with a PPARA-overexpressing plasmid in AnoR PC-3 cells. (**I**) Western blot of indicated protein level. (**J**) Western blot of AIFM2 protein level in experimental group, and luciferase reporter assay showing AIFM2 promoter activity in AnoR PC-3 cells. Data are expressed as representative images or as the mean ± SD of three independent experiments. $*P < 0.05$; $**P < 0.01$; ns, not significant.

`

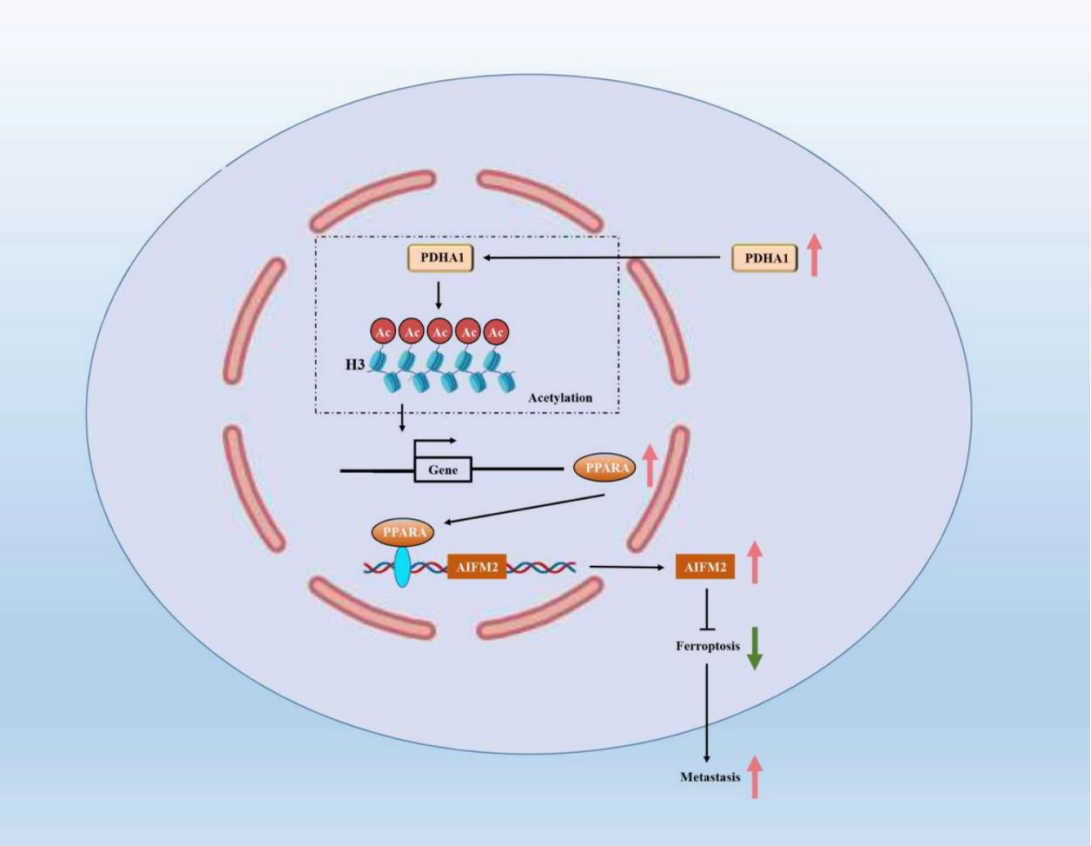

Fig.7 PDHA1 is highly expressed in anoikis resistance prostate cancer cells. Increased entry of PDHA1 into the nucleus of anoikis resistance causes an elevation of H3K9Ac level, which in turn induces the expression of PPARA that promotes the expression of AIFM2 through transcriptional activation, thereby inhibiting ferroptosis to promote metastasis.